HHS Public Access

Author manuscript

Wiley Interdiscip Rev Nanomed Nanobiotechnol. Author manuscript; available in PMC 2018 June 06.

Published in final edited form as:

Wiley Interdiscip Rev Nanomed Nanobiotechnol. 2018 May ; 10(3): e1496. doi:10.1002/wnan.1496.

Two decades of dendrimers as versatile MRI agents: a tale with and without metals

Michael T. McMahon[1,2,*] and **Jeff W. M. Bulte**[1,2,3,4,5,6,*]

[1]The Russell H. Morgan Department of Radiology and Radiological Science, Division of MR Research, The Johns Hopkins University School of Medicine, Baltimore, MD, USA

[2]F. M. Kirby Research Center for Functional Brain Imaging, Kennedy Krieger Institute, Baltimore, MD, USA

[3]Cellular Imaging Section and Vascular Biology Program, Institute for Cell Engineering, The Johns Hopkins University School of Medicine, Baltimore, MD, USA

[4]Department of Biomedical Engineering, The Johns Hopkins University School of Medicine, Baltimore, MD, USA

[5]Department of Oncology, The Johns Hopkins University School of Medicine, Baltimore, MD, USA

[6]Department of Chemical & Biomolecular Engineering, The Johns Hopkins University Whiting School of Engineering, Baltimore, MD, USA

Abstract

Dendrimers or dendritic polymers are a class of compounds with great potential for nanomedical use. Some of their properties, including their rigidity, low poly-dispersity and the ease with which their surfaces can be modified make them particularly well suited for use as MRI diagnostic or theranostic agents. For the past 20 years, researchers have recognized this potential and refined dendrimer formulations to optimize these nanocarriers for a host of MRI applications, including blood pool imaging agents, lymph node imaging agents, tumor-targeted theranostic agents and cell tracking agents. This review summarizes the various types of dendrimers according to the type of MR contrast they can provide. This includes the metallic T_1, T_2 and paraCEST imaging agents, and the non-metallic diaCEST and fluorinated (^{19}F) heteronuclear imaging agents.

THE DAWN OF DENDRIMERS

Dendrimers or dendritic polymers are one of the major classes of polymers. Unlike the first three major classes of polymers: linear, cross-linked and branched, dendrimers are polymer molecules which are synthesized with a central core and monomers which branch out radially from this core in a way that resembles a tree, hence their name (tree = δε̄νδον or dendron in Greek). They are sometimes also referred to as arborols (tree = arbor in Latin).

*Correspondence to: mtmcmaho@gmail.com or jwmbulte@mri.jhu.edu.

M.T.M and J.W.M.B. are co-founders of and hold an equity ownership in the startup company SenCEST, LLC. Some of the methodologies reviewed in this paper may ultimately become part of a SenCEST product. This arrangement has been reviewed and approved by the Johns Hopkins University in accordance with its conflict of interest policies.

The organic syntheses which led to dendrimers with their spherical architecture and easily functionalized surface were first conducted over 30 years ago,[1–3] with key early contributions to the field from the groups of Vogtle,[1] Denkewalter,[3] Tomalia,[2] and Newkome.[4] Dendrimers are synthesized in steps, so that the resulting structures generated have a relatively narrow polydispersity. Because the methods are similar to solid-phase peptide or oligonucleotide synthesis, it is readily possible to produce quantities appropriate for commercial use. This narrow polydispersity is also an important characteristic for pharmaceutical development, as it is desirable for manufactured drugs to be composed of a single, defined species whose identity and stability can be specified using techniques that are validated.[5] A number of different types of monomers are important building blocks for dendrimers including polyaminoamine (PAMAM), poly-L-lysine (PLL), 2,2-bis-methylolpropionic acid (bis-MPA), phenoxymethyl (methylhydrazone) (PMMH) and polypropylimine [PPI, also known as diaminobutane (DAB)]. At this time, there are five main types of dendrimers which are commercially available: Tomalia-type PAMAM dendrimers, Denkewalter-type PLL dendrimers, Hult-type bis-MPA dendrimers, Majoral/ Caminade-type phosphorous dendrimers and Vogtle/Meijer/ Multhaupe-type PPI dendrimers (Figure 1). Because of their special properties and features, dendrimers have been of great interest to the field of nanomedicine.

Based on sensitivity considerations, there has been a longstanding interest in the development of macromolecular Magnetic Resonance (MR) imaging agents as multiple contrast-providing entities can be coupled to a single macromolecule to enhance the sensitivity of detection.[6] One of the challenges for early polymeric Magnetic Resonance Imaging (MRI) agents based on albumin, poly-lysine (PL) and dextran macromolecules was that the relaxivities were not large. However, as Wiener et al. showed in the 1990s, Tomalia-type Starburst PAMAM dendrimers can be prepared as high sensitivity MR contrast agents.[7] This was followed by Weinmann and coworkers who showed that the Denkewalter-type PL-based dendrimers could be prepared as high sensitivity agents as well.[8,9] The general structures of these two dendrimer ‘molecular’ scaffolds first utilized as MRI agents are shown in Figure 1. One of the key observations made is that the relaxivities using albumin, PL and dextran were relatively low due to their floppiness. Dendrimers, however, which form a more rigid structure, displayed high relaxivity when paramagnetic ions were attached.[7] These initial studies spurred a number of others, as dendrimers have unique properties as MRI agents because of their adaptable nature, ease of conjugation to a wide variety of diagnostic agents, tunable pharmacokinetic profile, enhanced relaxivities when gadolinium is conjugated and potential for targeting. As a result, this platform has become increasingly popular, with a wide range of dendrimer scaffolds rendered MR-visible through a variety of contrast mechanisms.

Dendrimers can be prepared using a number of different core topologies (Figure 2). Due to the diversity of cores and monomers from which the dendrimer can be assembled, a number of different synthetic strategies have been developed. Reiterative synthesis is used in the assembly, with each addition of monomer layers creating a new generation (G). For each new generation, the number of terminal groups doubles from 8 terminal groups for G = 1 to 64 for G = 4 Starburst PAMAM dendrimer. Dendrimers are prepared using iterative synthesis strategies which are either convergent or divergent. The divergent strategy involves

reactions at the periphery of the dendrimer for each step, which results in exponential-like growth with increasing polydispersity for each step. For the convergent route, ‘dendrons’ (dendrimer branches attached to the core) are prepared separately, and then attached to the final core. This synthetic route enables the preparation of ‘Janus’ dendrimers, i.e., dendrimers with two or more terminal groups that face a different direction on the surface (Figure 2). These dendrimers are named after the Roman god Janus, which is usually depicted as having two faces, with one looking to the future and one to the past. Amphiphilic Janus dendrimers with hydrophilic and hydrophobic surfaces can self-assemble into larger dendrisomes (Figure 2). Of the different types of commercially available dendrimers, the Starburst PAMAM dendrimers are most commonly used. Aside from a simple purchase, their advantages include the availability of a range of generations (G1 to G9) and a range of different terminal groups (such as amino, carboxylate, amidoethanol, amidoethylethanolamine, and succinamic acid) on the surface. An important feature for imaging is the large increase in density of surface groups as the generation of the dendrimer increases. This allows high generation dendrimers to become more spherical and provide a very high concentration of MR agents or targeting moieties on the surface.[10] The terminal group charge impacts the route of intracellular transport,[11,12] cytotoxicity,[13–17] and the solubility of the dendrimer. All of these are design considerations for optimizing the interactions between the dendrimer and its microenvironment within the tissue to be imaged with MRI. Since their inception some 30–40 years ago, dendrimers have now seen a plethora of MRI applications over the last two decades (Figure 3).

PARAMAGNETIC GADOLINIUM DENDRIMERS

Since gadolinium has seven unpaired electrons, it is a paramagnetic agent with one of the highest relaxivities, depending on NMR frequency (field strength).[18] Wiener et al. were the first to describe the use of a PAMAM dendrimer as a nanocarrier for gadolinium as MR contrast agent.[7] Due to the increase in the rotational correlation time of the large dendrimer molecules, the relaxivity per Gd(III) ion of the dendrimer compared to that of a single Gd(III) chelate was enhanced up to sixfold. These factors are more than twice those observed for analogous metal-chelate conjugates formed with serum albumins, PL, or dextran. Due to their prolonged half-life (up to 200 min), the dendrimer-based agents provided excellent contrast on 3D time-of-flight MR angiograms (Figure 4).

Higher generation (G = 5, G = 7, G = 9, and G = 10) PAMAM dendrimers have been conjugated with the bifunctional chelate 2-(4-isothiocyanatobenzyl)-1,4,7,10-tetraazacyclododecane-N,N8,N″,N‴-tetraacetate (p-SCN-Bz-DOTA).[19] DOTA (1,4,7,10-tetraazacy-clododecane-1,4,7,10-tetraacetic acid) is a macrocycle with better stability kinetics than DTPA. These high generation dendrimers were initially developed as a contrast platform for targeted molecular imaging, given their anticipated high relaxivities. At 20 MHz, T_1 relaxivity increased from 30 mM^{-1} s^{-1} for G = 5 to 35 mM^{-1} s^{-1} for G = 7 dendrimers, reaching a plateau at 36 mM^{-1} s^{-1} for G = 9 and G = 10 dendrimers. Although the ion relaxivity thus did not increase and was minimally dependent on frequency, given their higher number of Gd-DOTA groups, the total molecular relaxivities increased from 2880 mM^{-1} s^{-1} to 66,960 mM^{-1} s^{-1} for the G = 5 and G = 10 dendrimer, respectively.[10,19]

The first targeted Gd-dendrimers that were used contained folate for selective imaging of high affinity folate receptor (hFR)-overexpressing tumor cells.[20] Treatment of tumor cells that expressed the hFR with gadolinium complexes of the folate-conjugated polymeric chelate increases the longitudinal relaxation rate by 110%. This increase was inhibited by an excess of free folic acid, demonstrating specificity. Using a ^{153}Gd isotope in lieu of the nonradioactive, conventional ^{157}Gd isotope, tumor uptake and tissue biodistribution was quantified for hFR-positive and -negative ovarian tumor xenografts.[21] The hFR-positive tumors accumulated 3.6 ± 2.8% of the injected dose/g tissue, whereas the counts in hFR-negative tumors were near background level. A different tumor targeting approach was the use of activatable cell-penetrating peptides (ACPPD). Twenty-four hours after injection of Gd-dendrimer-ACPPD in mice, orthotopic breast cancer cells enhanced 57% compared to 25% for a single Gd-chelate.[22] In another study, Arg-Gly-Asp-Phe-Lys(mpa)) (RGD) peptides have been used as targeting moieties combined with a multimodal gadolinium dendrimer contrast agent, entrapped with gold nanoparticles. This agent was able to visualize alpha V beta 3-integrin-overexpressing tumor cells on both Computed Tomography (CT) and MRI.[23] Another study employed a cyclic peptide which specifically binds to fibrin-fibronectin to enhance tumor uptake.[24] However, specific targeting of such dual-mode dendrimers may not be a prerequisite, as nontargeted gadolinium/ gold dendrimers have been showed to accumulate selectively in tumor cells *in vivo* as well,[25] presumably through an enhanced permeability retention effect seen in other instances.[26] An interesting feature of targeted gadolinium dendrimers is that they can be used as therapeutic agents based on neutron capture therapy (NCT). In this case, the targeted dendrimers are irradiated with an external neutron beam. The dendrimer-bound gadolinium then generates Auger electrons which are highly cytotoxic to tumor cells. This concept, which requires a high accumulation of gadolinium in target tissue, has been tested on SHIN3 ovarian carcinomas.[27] Selective filtration and retention by the lymphatic system has been exploited to enhance lymph ducts and lymph nodes on MRI following injection of gadolinium dendrimers.[28–31] Additional examples of specific targeting of gadolinium dendrimers to tumor cells include their conjugation to anti-tumor-specific antibodies.[32,33] Further applications using targeted dendrimers are rapidly expanding, based on the proven success of this strategy.

The synthesis of Gd-dendrimers and their analogs has recently been further optimized and refined. These include Gadomer-17 which is based on a PLL-dendrimer scaffold,[8,34,35] glycodendrimers,[36] and self-assembled dendritic-like nanoparticles.[37] The latter is an example of supramolecular engineering which may allow disassembly of the construct, facilitating the incorporation of other agents for multimodal imaging and conjugation of targeting moieties. One of the challenges in preparing dendrimers is the number of impurities from under-reacted intermediates which can ultimately hamper their approval. This is a general problem for macromolecular agents, and has led some groups to develop alternative gadolinium chelates such as Ablavar (gadofosveset) which binds to human serum albumin resulting in an increase in blood half-life and rotational correlation time. This agent possesses the purity attainable for small molecule MRI contrast agents while exhibiting relaxivities attainable by the macromolecular agents, facilitating regulatory approval.[38] Because of these challenges, the preparation of the contrast agent Gadomer-17 was a very impressive display of process chemistry in that Bayer-Schering AG was able to produce high

purity dendrimer agents on a multi-kiloscale which allowed this product to be administered to patients.[9,39] A few studies have explored the development of Gd-dendrimers as agents for sensing the microenvironment as well, so called 'smart' or 'responsive' agents. One example is the use of Ca^{2+}-sensing Gd-PAMAM dendrimers, that were successfully used to report on local calcium fluctuations in rat cerebral cortex.[40] All these examples demonstrate the versatility of dendritic structures for their use in MRI.

PARAMAGNETIC MANGANESE DENDRIMERS

Manganese (Mn II) exhibits anomalous relaxation behavior, and at higher fields can exhibit relaxivities that are higher than gadolinium.[18] A manganese-chelating hexameric dendrimer containing six tyrosine-derived [Mn(EDTA)(H2 O)](2−) moieties exhibited relaxivities ranging from 8.2 to 3.8 mM^{-1} s^{-1} from 0.47 to 11.7 T, sixfold higher on a per molecule basis compared to a single moiety.[41] As a vascular agent, blood clearance was fast and elimination occurred through both the renal and hepatobiliary routes.

To construct a targeted manganese-dendrimer, a large G = 8 dendrimer was conjugated to an antibody specific for malondialdehyde (MDA)-lysine epitopes. This target is one of the oxidation-specific epitopes (OSE) that is expressed in atherosclerotic plaques. An enhancement >60% could be observed compared to the untargeted counterpart.[42] Other modalities beyond MRI have been further studied. As an example, a dual-mode agent for combined CT/MRI was described based on hyaluronic acid-modified, multifunctional nanoparticles.[43] To this end, G = 5 Mn-dendrimers were first complexed to fluorescein isothiocyanate and hyaluronic acid. Gold nanoparticles were then entrapped within the above raw product, and the CD44 receptor-mediated endocytosis pathway was exploited to image targeted hepatocellular carcinoma cells in mice.

PARAMAGNETIC DYSPROSIUM DENDRIMERS

The above-described dendrimers were developed as T_1 agents to provide positive contrast. A different approach is to develop dendrimers as T_2 agents to provide negative contrast. Among the T_2 agents in general, superparamagnetic iron oxide (SPIO) nanoparticles (see *Superparamagnetic Dendrimers* section) and the lanthanide dysprosium have been most widely used. Dy(III) (G = 5) dendrimers were explored for their relaxation properties at various magnetic fields.[44] As expected, the T_1 relaxivities were very low, between 0.1 and 0.2 mM^{-1} s^{-1}. No major differences were found between the Dy-dendrimer and Dy-DOTA and Dy-DTPA single chelates. At lower fields (0.05–0.1 T), the $1/T_2$ was identical to $1/T_1$. Surprisingly, at higher fields, the $1/T_2$ increased quadratically with field strength, with a strong dependence on temperature (Figure 5). The field-dependent component of $1/T_2$ was up to three times higher for the Dy-DOTA-based dendrimer compared with the single chelate molecules. The results are well-explained by the inner sphere theory of susceptibility effects, also known as Curie spin relaxation. The large temperature dependence that was observed was indicative that the dominant mechanism of relaxation is the contact interaction effect, with the proton residence time or τ_m as the primary time constant. It was then suggested[44] that exploiting this relaxation mechanism enabled the creation of high-relaxivity selective T_2 contrast agents (i.e., high R2/R1 ratios) which could be further improved using

certain nonionic structural chelates such as bis(methyl)amide(BMA)-DTPA complexes which are associated with unusually long τ_m values. Indeed, subsequent studies proved this to be feasible.[44] Further work using single Dy(III) chelates with and without binding to a macromolecule (albumin) demonstrated that a longer rotational correlation time further enhances T_2 relaxivity,[45] similar to the enhancements observed for the macromolecular dendrimers themselves. Recently, after a lag of some 15+ years, there has been renewed interest in developing high relaxivity T_2 agents using dendrimerization of Dy(III) chelates while manipulating the water exchange rate.[46]

SUPERPARAMAGNETIC DENDRIMERS

The first use of SPIO nanoparticles complexed to dendrimers was described in 2001.[47] These magneto-dendrimers proved to be negative contrast agents with extremely high R2/R1 ratios. Here, the dendrimers were used as a stabilizer and coating agent for the SPIO cores grown from ferrous ions in solution in the presence of dendrimers[48] (Figure 6). This synthetic process is different from conventional SPIO synthesis for producing MR contrast agents, where the dextran acts as a nanoparticle coating agent and stabilizer instead of the dendrimer.[49] The use of magnetodendrimers has found major applications in MRI cell tracking,[50–53] and laid the groundwork for the subsequent use of (commercial) transfection agents or other polycation coatings[54,55] that quickly succeeded the use of magnetodendrimers as cell labeling agents due their cumbersome and time-consuming synthesis. Using commercial SPIO preparations, this method of (poly)cationic complexing is still the standard cell labeling practice in use today. Magnetodendrimers can also be prepared as targeted agents, i.e., using folate again but then combined with Au to become dual CT/MRI-targeted tumor agents.[56]

CEST DENDRIMERS

Chemical exchange saturation transfer (CEST) is an MR contrast mechanism that holds great promise.[57–64] CEST allows amplified detection of low concentration molecules by applying selective saturation pulses on resonance with the exchangeable protons present in these molecules. If these protons possess suitable exchange rates, a large amplification of their concentration can be transferred to water in the form of water signal loss, allowing molar changes in water signal from micromolar to millimolar concentrations of exchangeable protons and production of high contrast images. In addition, the capabilities of CEST imaging have been extended from water imaging to hyperpolarized xenon imaging, through development of suitable cage structures which allow detection of the cages through saturation transfer from the inside to the outside of the cages with the hyperpolarization and exchange allowing high sensitivity detection of these cages.[65,66] For both water-and xenon-based CEST, the usage of selective pulses prior to the imaging sequence for ‘switching on’ the contrast results in very different features from other MRI agents. For example, CEST agents can be designed with exchangeable protons resonating at a number of different frequencies, allowing the production of what has been called multicolor[67,68] or multi-frequency spectral[69,70] MR contrast. This feature makes CEST agents analogous to the use of frequency-specific multicolor optical imaging agents. In addition, chemical exchange is very dependent on the environment, and as a result a number of environmental sensors have

been developed for detecting changes in pH, ion concentration, enzyme concentration and metabolite concentration.[71–80] CEST agents can be divided into two classes, diamagnetic CEST (diaCEST) agents and paramagnetic CEST (paraCEST) agents, based on the magnetic properties of these agents. Both classes of CEST agents have been combined with dendrimers as MRI agents.

Diamagnetic CEST (diaCEST) Dendrimers

Why is there an interest in developing diaCEST dendrimers? Gadolinium-based contrast agents (GBCAs) have been the most widely used tracers for MRI with GBCA administered to approximately one-quarter of all patients undergoing MRI scans, or over 100 million patients over the past 25 years.[81,82] Hence, many initial MRI studies have used gadolinium-containing dendrimers. While the clinical small molecule GBCAs were designed to be nearly completely excreted in urine after i.v. injection, it was found that there is a relationship between patients with impaired kidney function who were administered GBCA and the occurrence of nephrogenic systemic fibrosis.[83–86] In addition, there is now clear evidence of accumulation of gadolinium in the brain (dentate nucleus and globus pallidus) and bones of patients despite a normal renal function.[82,87–90] These findings have stimulated interest in alternative MRI agents which do not employ gadolinium or other lanthanides. One clear alternative is the use of nonmetallic diaCEST agents, with the first patient studies now being performed with two diaCEST agents: glucose and iopamidol.[91–93] Because of limitations in the sensitivity of detection for diaCEST agents, there has been a longstanding interest in preparing nanocarrier CEST agents,[71,94–96] with dendrimers being an attractive candidate for this purpose.

PAMAM dendrimers which possess many primary amines were the first diamagnetic dendrimers shown to be detectable with CEST MRI.[97] A detailed investigation of the CEST properties of PAMAM dendrimers has been performed, and it was found that the proton exchange rate (k_{ex}) for amine-capped PAMAM dendrimers was too slow (k_{ex} = 30–300 s^{-1} for pH 6–7.3) and the chemical shift difference with water ($\Delta\omega$) too small for obtaining sufficient contrast at neutral pH values.[98] Since then, a large number of diamagnetic compounds have been identified which create CEST contrast based on their labile protons, including glucose,[99,100] L-arginine,[101] creatine,[102–104] glutamate,[105–107] iopamidol,[108,109] barbituric acid,[95] imidazole derivatives,[110] thymidine derivatives[111], and others. With the goal of identifying compounds which produce the strongest CEST contrast using a 3T clinical scanner, it was determined that salicylic acid (SA) derivatives possess labile OH protons with large chemical shifts from water (≥6 ppm) and exchange rates well-suited for detection.[112] Similarly, anthranilic acid derivatives have been identified.[113] Experimental and density functional theory investigations were performed to identify which factors play a role in obtaining a large $\Delta\omega$ and optimal k_{ex}.[114,115] Using this approach, a salicylic acid methyl ester (SAME) was developed and conjugated to PAMAM dendrimers.[116] After infusion into mice bearing brain tumors, the CEST contrast induced by these SA dendrimers persisted for ~90 min (Figure 7). SA dendrimer agents have potential for a variety of applications, including their use as theranostic agents.

Paramagnetic CEST (paraCEST) Dendrimers

One of the disadvantages of diaCEST agents is the relatively small range of $\Delta\omega$ found in diamagnetic compounds. This limitation in $\Delta\omega$ impacts their detectability, as the exchange rate must fall within the slow to intermediate exchange regime for saturation transfer to occur so that $k_{ex} \leq \Delta\omega$. Larger k_{ex} values result in larger CEST amplification factors, as fast exchange increases the number of exchange events that occur during the saturation pulse train. One strategy to increase $\Delta\omega$ is to incorporate a paramagnetic metal ion (shift agent) into the agent, which alters the frequencies of the labile protons with as result an increased separation from bulk water.[117,118] For these paraCEST agents, the relationship between proton frequencies and CEST contrast is complicated due to the occurrence of line broadening from electron spin relaxation rates, so that the metal ions and coordination geometries must be properly selected.[119,120] ParaCEST agents can be further divided into two categories with different types of exchangeable protons: water-based paraCEST agents, where water is weakly bound to a metal ion with these water protons paramagnetically shifted from bulk water and proton-based paraCEST agents, where exchanging amide, amine or hydroxyl protons near the metal ion exhibit a paramagnetic shift. As water is bound along the axis of symmetry for many complexes, the magnitude of the paramagnetic shift is typically much larger (50–600 ppm) than for proton-based agents (3–80 ppm).[121] There are a number of metal ion complexes in both categories which have been developed for this purpose, with the majority of these employing lanthanides (Ln) because of their favorable electronic relaxation properties and the detailed knowledge that exists on the water exchange in Ln complexes.[58,121,122] A large percentage of paraCEST Ln complexes employ amide derivatives of DOTA as ligand because of the large stability constant of the DOTA-chelated lanthanides and the large paramagnetic shifts that can produced at high field, up $\Delta\omega = 600$ ppm[121] For comparison, a maximum value of only ~12 ppm can be achieved for dia-CEST agents.[114] Metal ion complexes have also been prepared with the transition metals iron, nickel, and cobalt chelated with macrocycles containing heterocyclic amine donor groups that display excellent CEST contrast at $\Delta\omega$ up to 135 ppm.[123]

ParaCEST agents, similar to diaCEST agents, have sensitivity limitations and as a result these agents have been incorporated to nanocarriers to improve their detectability.[96,124,125] The first dendrimer paraCEST agents were prepared through coupling Yb^{3+}-DOTAM complexes to a poly(propylene imine) dendrimer, with the resulting nanocarrier displaying a pH-sensitive CEST contrast at $\Delta\omega = -15$ ppm.[126] Eu^{3+}-DOTA-Gly has also been coupled to PAMAM dendrimers with $\Delta\omega = -55$ ppm, and accumulation of this agent in MCF-7 mammary carcinoma in mice could be demonstrated *in vivo* after i.v. injection.[127] In this study, the accumulation of a G = 2 and a G = 5 dendrimer was compared, with the larger dendrimer displaying less accumulation and a slower uptake in the tumor tissue. A second study was performed by the same group using a dual fluorescent/paraCEST PAMAM dendrimer for monitoring brain tumor uptake.[128] Eu^{3+}-DOTA-Gly and Dylight 680 were conjugated to G5-PAMAM dendrimers and administered i.v. to mice bearing U87 gliomas. CEST contrast could again be demonstrated, which was primarily confined to the rim of the brain tumor. Similar to diaCEST dendrimers, paraCEST dendrimer agents have potential for a variety of diagnostic applications, with or without the use of co-conjugated therapeutic agents.

FLUORINATED DENDRIMERS

^{19}F is an MRI detectable spin ½ nucleus which is 100% naturally abundant with the highest gyromagnetic ratio (94% of ^{1}H) of all heteronuclei.[129] ^{19}F imaging agents are now entering the clinic[130,131] because of their advantage of absolute quantification by direct detection,[132] compared to indirect detection of the proton-based contrast agents. Since there is no background signal in biological tissue, one can perform 'hot spot' imaging.[133] Due to the lack of contrast, fluorinated agents should be referred to as MRI 'tracers' (analogous to the term radioactive 'tracers' in nuclear medicine) instead of contrast agents. The design of proper ^{19}F imaging agents is therefore much more simple and straightforward than that of CEST or other proton-based contrast agents: to create a nanocarrier with a very large number of ^{19}F atoms that are chemically equivalent to maximize their detection. Since a limitation of hot spot ^{19}F MRI is its low sensitivity, dendrimers have been naturally explored as a high payload carrier.

^{19}F-doped dendrimers have been prepared since the late 1990s for extractions and for catalysis.[134,135] The first polymeric fluorine agents specifically designed for MRI detection were small Janus dendrimers, which produced a single ^{19}F NMR line.[136] Later on, much larger fluorodendrimers were prepared using convergent synthesis methods, with larger number of near completely chemically equivalent fluorine atoms per dendrimer, and polydispersity indexes that are much lower than G = 2 PAMAM dendrimers.[137,138] While current *in vivo* studies using fluorodendrimers are limited,[139] these hot spot MRI agents should be particularly useful for applications that strongly benefit from molecular quantification. Recent refinements of synthetic procedures include pseudosymmetrical fluorine positioning,[140] self-sorting and co-assembly of fluorinated Janus dendrimers into dendrimersomes.[141] A fluorinated dendron-cyanine dye-conjugated dual-mode agent for combined optical near-infrared imaging and ^{19}F MRI has also been described, that combines the high sensitivity of optical imaging with that of ^{19}F MRI for quantification.[142]

OPPORTUNITIES AND LIMITATIONS

Aside from the presence of paramagnetic and lanthanide metals, which is not an issue for the use of dia-CEST dendrimers, future regulatory approval for clinical use of (high-generation) dendrimers will also depend on the eventual fate of the dendrimer scaffold itself. While these organic compounds in theory are expected to break down into parts that can be metabolized, little is known about their overall biodegradation or excretion once retained in the body for prolonged times. Low- to medium-generation dendrimers (G < 6) are largely excreted by the kidney after i.v. injection. However, in addition to size, the surface zeta potential may also become a contributing factor. Cationic ^{125}I-labeled PAMAM dendrimers (G = 3 and 4) are cleared rapidly from the circulation (<2% of the recovered dose is present in blood after 1 h), while anionic PAMAM dendrimers (G = 2.5, 3.5, and 5.5) showed longer circulation times (~20–40% of the recovered dose present in blood after 1 h), demonstrating generation-dependent clearance rates.[143] In addition to this, polycationic dendrimers can display considerable toxicity.[17] Furthermore, the clearance rate also depends on core composition. PPI dendrimers agents clear more rapidly from the body than PAMAM dendrimers for the same number of branches[144] and bis-MPA dendrimers will degrade

readily due to ester hydrolysis.[145,146] Therefore, it seems plausible that PAMAM-G2, PPI-G3, PPI-G2, bis-MPA-G2, and bis-MPA-G3 dendrimers, given their relatively rapid excretion, are most likely to be used further for clinical translation, with a compromise in terms of target sensitivity compared to higher generation dendrimers.

CONCLUSIONS

Over the last two decades, we have witnessed an explosion of studies employing dendrimers as MRI agents, with over 400 papers published (Figure 8(a)). These papers now receive no less than 2800 citations a year (Figure 8(b)), which shows the overall impact of this work. Virtually any material that can provide MR contrast has been incorporated into dendrimers and evaluated. All of these studies have been proof-of-principle, with only Gadomer-17 having been tested in man.[147] Detailed toxicity studies have been lacking, and thorough side-by-side biodistribution studies have been few. Nevertheless, multiple studies have demonstrated the intrinsic high payload capability of dendrimers as nanocarriers for imaging agents, which, for MRI, is a necessary component for imaging beyond the vessel wall.

References

1. Buhleier E, Wehner W, Vogtle F. Cascade-chain-like and nonskid-chain-like syntheses of molecular cavity topologies. Synthesis (Stuttg). 1978; 2:155–158.
2. Tomalia DA, Baker H, Dewald J, Hall M, Kallos G, Martin S, Roeck J, Ryder J, Smith P. A new class of polymers –starburst-dendritic macromolecules. Polym J. 1985; 17:117–132.
3. Denkewalter, RG., Kolc, J., Lukasavage, WJ. Macromolecular highly branched homogeneous compound based on lysine units. 1981. Available at: http://www.google.com.au/patents/US4289872
4. Newkome GR, Yao ZQ, Baker GR, Gupta VK. Micelles. 1. Cascade molecules: a new approach to micelles – A 27-arborol. J Org Chem. 1985; 50:2003–2004.
5. Duncan R, Izzo L. Dendrimer biocompatibility and toxicity. Adv Drug Deliv Rev. 2005; 57:2215–2237. [PubMed: 16297497]
6. Brasch RC. Rationale and applications for macromolecular GD-based contrast agents. Magn Reson Med. 1991; 22:282–287. [PubMed: 1725917]
7. Wiener EC, Brechbiel MW, Brothers H, Magin RL, Gansow OA, Tomalia DA, Lauterbur PC. Dendrimer-based metal-chelates – a new class of magnetic resonance imaging contrast agents. Magn Reson Med. 1994; 31:1–8. [PubMed: 8121264]
8. Dong Q, Hurst DR, Weinmann HJ, Chenevert TL, Londy FJ, Prince MR. Magnetic resonance angiography with gadomer-17 – an animal study original investigation. Invest Radiol. 1998; 33:699–708. [PubMed: 9766055]
9. Raduchel B, Schmitt-Willich H, Platzek J, Ebert W, Frenzel T, Misselwitz B, Weinmann HJ. Synthesis and characterization of novel dendrimer-based gadolinium complexes as MRI contrast agents for the vascular system. Abstracts of Papers of the American Chemical Society. 1998; 216:U900.
10. Bryant LH Jr, Jordan EK, Bulte JW, Herynek V, Frank JA. Pharmacokinetics of a high-generation dendrimer-Gd-DOTA. Acad Radiol. 2002; 9(suppl 1):S29–S33. [PubMed: 12019888]
11. Perumal OP, Inapagolla R, Kannan S, Kannan RM. The effect of surface functionality on cellular trafficking of dendrimers. Biomaterials. 2008; 29:3469–3476. [PubMed: 18501424]
12. Kitchens KM, El-Sayed MEH, Ghandehari H. Transe-pithelial and endothelial transport of poly(amidoamine) dendrimers. Adv Drug Deliv Rev. 2005; 57:2163–2176. [PubMed: 16289433]
13. Agashe HB, Dutta T, Garg M, Jain NK. Investigations on the toxicological profile of functionalized fifth-generation poly(propylene imine) dendrimer. J Pharm Pharmacol. 2006; 58:1491–1498. [PubMed: 17132212]

14. Jain K, Kesharwani P, Gupta U, Jain NK. Dendrimer toxicity: let's meet the challenge. Int J Pharm. 2010; 394:122–142. [PubMed: 20433913]
15. Kolhatkar RB, Kitchens KM, Swaan PW, Ghandehari H. Surface acetylation of polyamidoamine (PAMAM) dendrimers decreases cytotoxicity while maintaining membrane permeability. Bioconjug Chem. 2007; 18:2054–2060. [PubMed: 17960872]
16. Chen HT, Neerman MF, Parrish AR, Simanek EE. Cytotoxicity, hemolysis, and acute *in vivo* toxicity of dendrimers based on melamine, candidate vehicles for drug delivery. J Am Chem Soc. 2004; 126:10044–10048. [PubMed: 15303879]
17. Brazeau GA, Attia S, Poxon S, Hughes JA. *In vitro* myotoxicity of selected cationic macromolecules used in non-viral gene delivery. Pharm Res. 1998; 15:680–684. [PubMed: 9619774]
18. Vymazal J, Bulte JW, Frank JA, Di Chiro G, Brooks RA. Frequency dependence of MR relaxation times. I. Paramagnetic ions. J Magn Reson Imaging. 1993; 3:637–640. [PubMed: 8347957]
19. Bryant LH Jr, Brechbiel MW, Wu C, Bulte JW, Herynek V, Frank JA. Synthesis and relaxometry of high-generation (G = 5, 7, 9, and 10) PAMAM dendrimer-DOTA-gadolinium chelates. J Magn Reson Imaging. 1999; 9:348–352. [PubMed: 10077036]
20. Wiener EC, Konda S, Shadron A, Brechbiel M, Gansow O. Targeting dendrimer-chelates to tumors and tumor cells expressing the high-affinity folate receptor. Invest Radiol. 1997; 32:748–754. [PubMed: 9406015]
21. Konda SD, Wang S, Brechbiel M, Wiener EC. Biodistribution of a 153 Gd-folate dendrimer, generation = 4, in mice with folate-receptor positive and negative ovarian tumor xenografts. Invest Radiol. 2002; 37:199–204. [PubMed: 11923642]
22. Malone CD, Olson ES, Mattrey RF, Jiang T, Tsien RY, Nguyen QT. Tumor detection at 3 Tesla with an activatable cell penetrating peptide dendrimer (ACPPD-Gd), a T1 magnetic resonance (MR) molecular imaging agent. PLoS One. 2015; 10:e0137104. [PubMed: 26336058]
23. Chen Q, Wang H, Liu H, Wen S, Peng C, Shen M, Zhang G, Shi X. Multifunctional dendrimer-entrapped gold nanoparticles modified with RGD peptide for targeted computed tomography/magnetic resonance dual-modal imaging of tumors. Anal Chem. 2015; 87:3949–3956. [PubMed: 25768040]
24. Tan MQ, Ye Z, Lindner D, Brady-Kalnay SM, Lu ZR. Synthesis and evaluation of a targeted nano-globular dual-modal imaging agent for MR imaging and image-guided surgery of prostate cancer. Pharm Res. 2014; 31:1469–1476. [PubMed: 23471641]
25. Li K, Wen S, Larson AC, Shen M, Zhang Z, Chen Q, Shi X, Zhang G. Multifunctional dendrimer-based nanoparticles for *in vivo* MR/CT dual-modal molecular imaging of breast cancer. Int J Nanomedicine. 2013; 8:2589–2600. [PubMed: 23888113]
26. Kobayashi H, Reijnders K, English S, Yordanov AT, Milenic DE, Sowers AL, Citrin D, Krishna MC, Waldmann TA, Mitchell JB, et al. Application of a macromolecular contrast agent for detection of alterations of tumor vessel permeability induced by radiation. Clin Cancer Res. 2004; 10:7712–7720. [PubMed: 15570005]
27. Kobayashi H, Kawamoto S, Saga T, Sato N, Ishimori T, Konishi J, Ono K, Togashi K, Brechbiel MW. Avidin-dendrimer-(1B4M-Gd)254: a tumor-targeting therapeutic agent for gadolinium neutron capture therapy of intraperitoneal disseminated tumor which can be monitored by MRI. Bio-conjug Chem. 2001; 12:587–593.
28. Kobayashi H, Kawamoto S, Star RA, Waldmann TA, Tagaya Y, Brechbiel MW. Micro-magnetic resonance lymphangiography in mice using a novel dendrimer-based magnetic resonance imaging contrast agent. Cancer Res. 2003; 63:271–276. [PubMed: 12543772]
29. Kobayashi H, Kawamoto S, Sakai Y, Choyke PL, Star RA, Brechbiel MW, Sato N, Tagaya Y, Morris JC, Waldmann TA. Lymphatic drainage imaging of breast cancer in mice by micro-magnetic resonance lymphangiography using a nano-size paramagnetic contrast agent. J Natl Cancer Inst. 2004; 96:703–708. [PubMed: 15126607]
30. Kobayashi H, Kawamoto S, Brechbiel MW, Bernardo M, Sato N, Waldmann TA, Tagaya Y, Choyke PL. Detection of lymph node involvement in hematologic malignancies using micromagnetic resonance lymphangiography with a gadolinum-labeled dendrimer nanoparticle. Neoplasia. 2005; 7:984–991. [PubMed: 16331884]

31. Hama Y, Bernardo M, Regino CA, Koyama Y, Brechbiel MW, Krishna MC, Choyke PL, Kobayashi H. MR lymphangiography using dendrimer-based contrast agents: a comparison at 1.5 T and 3. 0 T. Magn Reson Med. 2007; 57:431–436. [PubMed: 17260373]
32. Kobayashi H, Wu C, Kim MK, Paik CH, Carrasquillo JA, Brechbiel MW. Evaluation of the *in vivo* biodistribution of indium-111 and yttrium-88 labeled dendrimer-1B4M-DTPA and its conjugation with anti-Tac monoclonal antibody. Bioconjug Chem. 1999; 10:103–111. [PubMed: 9893971]
33. Kobayashi H, Sato N, Saga T, Nakamoto Y, Ishimori T, Toyama S, Togashi K, Konishi J, Brechbiel MW. Monoclonal antibody-dendrimer conjugates enable radiolabeling of antibody with markedly high specific activity with minimal loss of immunoreactivity. Eur J Nucl Med. 2000; 27:1334–1339. [PubMed: 11007515]
34. Henderson E, Sykes J, Drost D, Weinmann HJ, Rutt BK, Lee TY. Simultaneous MRI measurement of blood flow, blood volume, and capillary permeability in mammary tumors using two different contrast agents. J Magn Reson Imaging. 2000; 12:991–1003. [PubMed: 11105041]
35. Misselwitz B, Schmitt-Willich H, Ebert W, Frenzel T, Weinmann HJ. Pharmacokinetics of Gadomer-17, a new dendritic magnetic resonance contrast agent. MAGMA. 2001; 12:128–134. [PubMed: 11390268]
36. Xiong Z, Wang Y, Zhu J, He Y, Qu J, Effenberg C, Xia J, Appelhans D, Shi X. Gd-chelated poly(propylene imine) dendrimers with densely organized maltose shells for enhanced MR imaging applications. Biomater Sci. 2016; 4:1622–1629. [PubMed: 27722500]
37. Besenius P, Heynens JL, Straathof R, Nieuwenhuizen MM, Bomans PH, Terreno E, Aime S, Strijkers GJ, Nicolay K, Meijer EW. Paramagnetic self-assembled nanoparticles as supramolecular MRI contrast agents. Contrast Media Mol Imaging. 2012; 7:356–361. [PubMed: 22539406]
38. Caravan P, Cloutier NJ, Greenfield MT, McDermid SA, Dunham SU, Bulte JWM, Amedio JC, Looby RJ, Supkowski RM, Horrocks WD, et al. The interaction of MS-325 with human serum albumin and its effect on proton relaxation rates. J Am Chem Soc. 2002; 124:3152–3162. [PubMed: 11902904]
39. Platzek, J., Schmitt-Willich, H. Synthesis and development of gadomer: a dendritic MRI contrast agent. In: Sessler, JL.Doctrow, SR.McMurry, TJ., Lippard, SJ., editors. Medicinal Inorganic Chemistry. Vol. 903. Washington, DC: American Chemical Society; 2005. p. 192-214.
40. Gunduz S, Nitta N, Vibhute S, Shibata S, Mayer ME, Logothetis NK, Aoki I, Angelovski G. Dendrimeric calcium-responsive MRI contrast agents with slow *in vivo* diffusion. Chem Commun (Camb). 2015; 51:2782–2785. [PubMed: 25383973]
41. Zhu J, Gale EM, Atanasova I, Rietz TA, Caravan P. Hexameric Mn(II) dendrimer as MRI contrast agent. Chemistry. 2014; 20:14507–14513. [PubMed: 25224391]
42. Nguyen TH, Bryant H, Shapsa A, Street H, Mani V, Fayad ZA, Frank JA, Tsimikas S, Briley-Saebo KC. Manganese G8 dendrimers targeted to oxidation-specific epitopes: *in vivo* MR imaging of atherosclerosis. J Magn Reson Imaging. 2015; 41:797–805. [PubMed: 24610640]
43. Wang R, Luo Y, Yang S, Lin J, Gao D, Zhao Y, Liu J, Shi X, Wang X. Hyaluronic acid-modified manganese-chelated dendrimer-entrapped gold nano-particles for the targeted CT/MR dual-mode imaging of hepatocellular carcinoma. Sci Rep. 2016; 6:33844. [PubMed: 27653258]
44. Bulte JW, Wu C, Brechbiel MW, Brooks RA, Vymazal J, Holla M, Frank JA. Dysprosium-DOTA-PAMAM dendrimers as macromolecular T2 contrast agents. Preparation and relaxometry. Invest Radiol. 1998; 33:841–845. [PubMed: 9818319]
45. Caravan P, Greenfield MT, Bulte JW. Molecular factors that determine Curie spin relaxation in dysprosium complexes. Magn Reson Med. 2001; 46:917–922. [PubMed: 11675643]
46. Soesbe TC, Ratnakar SJ, Milne M, Zhang S, Do QN, Kovacs Z, Sherry AD. Maximizing T2-exchange in Dy(3+)DOTA-(amide)X chelates: fine-tuning the water molecule exchange rate for enhanced T2 contrast in MRI. Magn Reson Med. 2014; 71:1179–1185. [PubMed: 24390729]
47. Bulte JW, Douglas T, Witwer B, Zhang SC, Strable E, Lewis BK, Zywicke H, Miller B, van Gelderen P, Moskowitz BM, et al. Magnetodendrimers allow endosomal magnetic labeling and *in vivo* tracking of stem cells. Nat Biotechnol. 2001; 19:1141–1147. [PubMed: 11731783]
48. Strable E, Bulte JWM, Moskowitz BM, Vivekanandan K, Allen M, Douglas T. Synthesis and characterization of soluble iron oxide-dendrimer composites. Chem Mater. 2001; 13:2201–2209.

49. Bulte JW, Kraitchman DL. Iron oxide MR contrast agents for molecular and cellular imaging. NMR Biomed. 2004; 17:484–499. [PubMed: 15526347]
50. Bulte JW, Douglas T, Witwer B, Zhang SC, Lewis BK, van Gelderen P, Zywicke H, Duncan ID, Frank JA. Monitoring stem cell therapy *in vivo* using magnetodendrimers as a new class of cellular MR contrast agents. Acad Radiol. 2002; 9(suppl 2):S332–S335. [PubMed: 12188266]
51. Walter GA, Cahill KS, Huard J, Feng H, Douglas T, Sweeney HL, Bulte JW. Noninvasive monitoring of stem cell transfer for muscle disorders. Magn Reson Med. 2004; 51:273–277. [PubMed: 14755651]
52. Bulte JW, Ben-Hur T, Miller BR, Mizrachi-Kol R, Einstein O, Reinhartz E, Zywicke HA, Douglas T, Frank JA. MR microscopy of magnetically labeled neurospheres transplanted into the Lewis EAE rat brain. Magn Reson Med. 2003; 50:201–205. [PubMed: 12815696]
53. Tunici P, Bulte JW, Bruzzone MG, Poliani PL, Cajola L, Grisoli M, Douglas T, Finocchiaro G. Brain engraftment and therapeutic potential of stem/progenitor cells derived from mouse skin. J Gene Med. 2006; 8:506–513. [PubMed: 16389624]
54. Frank JA, Zywicke H, Jordan EK, Mitchell J, Lewis BK, Miller B, Bryant LH Jr, Bulte JW. Magnetic intracellular labeling of mammalian cells by combining (FDA-approved) superparamagnetic iron oxide MR contrast agents and commonly used transfection agents. Acad Radiol. 2002; 9(suppl 2):S484–S487. [PubMed: 12188316]
55. Frank JA, Miller BR, Arbab AS, Zywicke HA, Jordan EK, Lewis BK, Bryant LH Jr, Bulte JW. Clinically applicable labeling of mammalian and stem cells by combining superparamagnetic iron oxides and transfection agents. Radiology. 2003; 228:480–487. [PubMed: 12819345]
56. Cai H, Li K, Li J, Wen S, Chen Q, Shen M, Zheng L, Zhang G, Shi X. Dendrimer-assisted formation of Fe_3O_4/Au nanocomposite particles for targeted dual mode CT/MR imaging of tumors. Small. 2015; 11:4584–4593. [PubMed: 26061810]
57. Liu GS, Song XL, Chan KWY, McMahon MT. Nuts and bolts of chemical exchange saturation transfer MRI. NMR Biomed. 2013; 26:810–828. [PubMed: 23303716]
58. Terreno E, Castelli DD, Aime S. Encoding the frequency dependence in MRI contrast media: the emerging class of CEST agents. Contrast Media Mol Imaging. 2010; 5:78–98. [PubMed: 20419761]
59. van Zijl PC, Yadav NN. Chemical exchange saturation transfer (CEST): what is in a name and what isn't? Magn Reson Med. 2011; 65:927–948. [PubMed: 21337419]
60. Hancu I, Dixon WT, Woods M, Vinogradov E, Sherry AD, Lenkinski RE. CEST and PARACEST MR contrast agents. Acta Radiol. 2010; 51:910–923. [PubMed: 20828299]
61. Hingorani DV, Bernstein AS, Pagel MD. A review of responsive MRI contrast agents: 2005–2014. Contrast Media Mol Imaging. 2015; 10:245–265. [PubMed: 25355685]
62. Vinogradov E, Sherry AD, Lenkinski RE. CEST: from basic principles to applications, challenges and opportunities. J Magn Reson. 2013; 229:155–172. [PubMed: 23273841]
63. Zaiss M, Bachert P. Chemical exchange saturation transfer (CEST) and MR Z-spectroscopy *in vivo*: a review of theoretical approaches and methods. Phys Med Biol. 2013; 58:R221–R269. [PubMed: 24201125]
64. McMahon, MT.Gilad, AA.Bulte, JWM., van Zijl, PCM., editors. Chemical Exchange Saturation Transfer Imaging: Advances and Applications. 1. Singapore: Pan Stanford Publishing; 2017. p. 479
65. Schroder L, Lowery TJ, Hilty C, Wemmer DE, Pines A. Molecular imaging using a targeted magnetic resonance hyperpolarized biosensor. Science. 2006; 314:446–449. [PubMed: 17053143]
66. Shapiro MG, Ramirez RM, Sperling LJ, Sun G, Sun J, Pines A, Schaffer DV, Bajaj VS. Genetically encoded reporters for hyperpolarized xenon magnetic resonance imaging. Nat Chem. 2014; 6:630–635.
67. McMahon MT, Gilad AA, DeLiso MA, Berman SM, Bulte JW, van Zijl PC. New "multicolor" polypeptide diamagnetic chemical exchange saturation transfer (DIACEST) contrast agents for MRI. Magn Reson Med. 2008; 60:803–812. [PubMed: 18816830]
68. Liu G, Moake M, Harel YE, Long CM, Chan KW, Cardona A, Jamil M, Walczak P, Gilad AA, Sgouros G, et al. *In vivo* multicolor molecular MR imaging using diamagnetic chemical exchange saturation transfer liposomes. Magn Reson Med. 2012; 67:1106–1113. [PubMed: 22392814]

69. Viswanathan S, Ratnakar SJ, Green KN, Kovacs Z, De Leon-Rodriguez LM, Sherry AD. Multi-frequency PARACEST agents based on europium(III)-DOTA-tetraamide ligands. Angew Chem. 2009; 48:9330–9333. [PubMed: 19894248]
70. Terreno E, Sanino A, Carrera C, Castelli DD, Giovenzana GB, Lombardi A, Mazzon R, Milone L, Visigalli M, Aime S. Determination of water permeability of paramagnetic liposomes of interest in MRI field. J Inorg Biochem. 2008; 102:1112–1119. [PubMed: 18329102]
71. Chan KWY, Liu G, Song X, Kim H, Yu T, Arifin DR, Gilad AA, Hanes J, Walczak P, van Zijl PCM, et al. MRI-detectable pH nanosensors incorporated into hydrogels for *in vivo* sensing of transplanted-cell viability. Nat Mater. 2013; 12:268–275. [PubMed: 23353626]
72. Bar-Shir A, Gilad AA, Chan KW, Liu G, van Zijl PC, Bulte JW, McMahon MT. Metal ion sensing using ion chemical exchange saturation transfer 19F magnetic resonance imaging. J Am Chem Soc. 2013; 135:12164–12167. [PubMed: 23905693]
73. Schroeder L, Meldrum T, Smith M, Lowery TJ, Wemmer DE, Pines A. Temperature response of (129) Xe depolarization transfer and its application for ultrasensitive NMR detection. Phys Rev Lett. 2008; 100:1–4.
74. Guo QN, Zeng QB, Jiang WP, Zhang XX, Luo Q, Zhang X, Bouchard LS, Liu ML, Zhou X. A molecular imaging approach to mercury sensing based on hyperpolarized Xe-129 molecular clamp probe. Chem Eur J. 2016; 22:3967–3970. [PubMed: 26792102]
75. Zhang J, Jiang WP, Luo Q, Zhang XX, Guo QN, Liu ML, Zhou X. Rational design of hyperpolarized xenon NMR molecular sensor for the selective and sensitive determination of zinc ions. Talanta. 2014; 122:101–105. [PubMed: 24720969]
76. Hingorani DV, Montano LA, Randtke EA, Lee YS, Cardenas-Rodriguez J, Pagel MD. A single diamagnetic catalyCEST MRI contrast agent that detects cathepsin B enzyme activity by using a ratio of two CEST signals. Contrast Media Mol Imaging. 2016; 11:130–138. [PubMed: 26633584]
77. Fernandez-Cuervo G, Sinharay S, Pagel MD. A Cata-lyCEST MRI contrast agent that can simultaneously detect two enzyme activities. Chembiochem. 2016; 17:383–387. [PubMed: 26693680]
78. Daryaei I, Ghaffari MM, Jones KM, Pagel MD. Detection of alkaline phosphatase enzyme activity with a CatalyCEST MRI biosensor. ACS Sens. 2016; 1:857–861.
79. Trokowski R, Ren J, Kalman FK, Sherry AD. Selective sensing of zinc ions with a PARACEST contrast agent. Angew Chem Int Ed Engl. 2005; 44:6920–6923. [PubMed: 16206314]
80. Ren JM, Trokowski R, Zhang SR, Malloy CR, Sherry AD. Imaging the tissue distribution of glucose in livers using a PARACEST sensor. Magn Reson Med. 2008; 60:1047–1055. [PubMed: 18958853]
81. Aime S, Caravan P. Biodistribution of gadolinium-based contrast agents, including gadolinium deposition. J Magn Reson Imaging. 2009; 30:1259–1267. [PubMed: 19938038]
82. Kanal E, Tweedle MF. Residual or retained gadolinium: practical implications for radiologists and our patients. Radiology. 2015; 275:630–634. [PubMed: 25942418]
83. Thomsen HS. Nephrogenic systemic fibrosis: a serious adverse reaction to gadolinium-1997–2006–2016. Part 1. Acta Radiol. 2016; 57:515–520. [PubMed: 26802069]
84. Rydahl C, Thomsen HS, Marckmann P. High prevalence of nephrogenic systemic fibrosis in chronic renal failure patients exposed to gadodiamide, a gadolinium-containing magnetic resonance contrast agent. Invest Radiol. 2008; 43:141–144. [PubMed: 18197066]
85. Marckmann P, Skov L, Rossen K, Dupont A, Damholt MB, Heaf JG, Thomsen HS. Nephrogenic systemic fibrosis: suspected causative role of gadodiamide used for contrast-enhanced magnetic resonance imaging. J Am Soc Nephrol. 2006; 17:2359–2362. [PubMed: 16885403]
86. Tombach B, Bremer C, Reimer P, Schaefer RM, Ebert W, Geens V, Heindel W. Pharmacokinetics of 1M gadobutrol in patients with chronic renal failure. Invest Radiol. 2000; 35:35–40. [PubMed: 10639034]
87. Kanda T, Ishii K, Kawaguchi H, Kitajima K, Takenaka D. High signal intensity in the dentate nucleus and globus pallidus on unenhanced T1-weighted MR images: relationship with increasing cumulative dose of a gadolinium-based contrast material. Radiology. 2014; 270:834–841. [PubMed: 24475844]

88. Errante Y, Cirimele V, Mallio CA, Di Lazzaro V, Zobel BB, Quattrocchi CC. Progressive increase of T1 signal intensity of the dentate nucleus on unenhanced magnetic resonance images is associated with cumulative doses of intravenously administered gadodiamide in patients with normal renal function, suggesting dechelation. Invest Radiol. 2014; 49:685–690. [PubMed: 24872007]

89. McDonald RJ, McDonald JS, Kallmes DF, Jentoft ME, Murray DL, Thielen KR, Williamson EE, Eckel LJ. Intracranial gadolinium deposition after contrast-enhanced MR imaging. Radiology. 2015; 275:772–782. [PubMed: 25742194]

90. Tweedle MF, Wedeking P, Kumar K. Biodistribution of radiolabeled, formulated gadopentetate, gadoteridol, gadoterate, and gadodiamide in mice and rats. Invest Radiol. 1995; 30:372–380. [PubMed: 7490190]

91. Xu X, Yadav NN, Knutsson L, Hua J, Kalyani R, Hall E, Laterra J, Blakeley J, Strowd R, Pomper M, et al. Dynamic glucose-enhanced (DGE) MRI: translation to human scanning and first results in glioma patients. Tomography. 2015; 1:105–114. [PubMed: 26779568]

92. Schuenke P, Koehler C, Korzowski A, Windschuh J, Bachert P, Ladd ME, Mundiyanapurath S, Paech D, Bickelhaupt S, Bonekamp D, et al. Adiabatically prepared spin-lock approach for T1rho-based dynamic glucose enhanced MRI at ultrahigh fields. Magn Reson Med. 2017; 78:215–225. [PubMed: 27521026]

93. Muller-Lutz A, Khalil N, Schmitt B, Jellus V, Pentang G, Oeltzschner G, Antoch G, Lanzman RS, Wittsack HJ. Pilot study of Iopamidol-based quantitative pH imaging on a clinical 3T MR scanner. MAGMA. 2014; 27:477–485. [PubMed: 24570337]

94. Castelli DD, Terreno E, Longo D, Aime S. Nanoparticle-based chemical exchange saturation transfer (CEST) agents. NMR Biomed. 2013; 26:839–849. [PubMed: 23784956]

95. Chan KW, Yu T, Qiao Y, Liu Q, Yang M, Patel H, Liu G, Kinzler KW, Vogelstein B, Bulte JW, et al. A diaCEST MRI approach for monitoring liposomal accumulation in tumors. J Control Release. 2014; 180:51–59. [PubMed: 24548481]

96. Aime S, Delli Castelli D, Terreno E. Highly sensitive MRI chemical exchange saturation transfer agents using liposomes. Angew Chem. 2005; 44:5513–5515. [PubMed: 16052647]

97. Goffeney N, Bulte JW, Duyn J, Bryant LH Jr, van Zijl PC. Sensitive NMR detection of cationic-polymer-based gene delivery systems using saturation transfer via proton exchange. J Am Chem Soc. 2001; 123:8628–8629. [PubMed: 11525684]

98. McMahon MT, Gilad AA, Zhou JY, Sun PZ, Bulte JWM, van Zijl PCM. Quantifying exchange rates in chemical exchange saturation transfer agents using the saturation time and saturation power dependencies of the magnetization transfer effect on the magnetic resonance imaging signal (QUEST and QUESP): pH calibration for poly-L-lysine and a star-burst dendrimer. Magn Reson Med. 2006; 55:836–847. [PubMed: 16506187]

99. Walker-Samuel S, Ramasawmy R, Torrealdea F, Rega M, Rajkumar V, Johnson SP, Richardson S, Goncalves M, Parkes HG, Arstad E, et al. *In vivo* imaging of glucose uptake and metabolism in tumors. Nat Med. 2013; 19:1067–1072. [PubMed: 23832090]

100. Chan KW, McMahon MT, Kato Y, Liu G, Bulte JW, Bhujwalla ZM, Artemov D, van Zijl PC. Natural D-glucose as a biodegradable MRI contrast agent for detecting cancer. Magn Reson Med. 2012; 68:1764–1773. [PubMed: 23074027]

101. Ward KM, Aletras AH, Balaban RS. A new class of contrast agents for MRI based on proton chemical exchange dependent saturation transfer (CEST). J Magn Reson. 2000; 143:79–87. [PubMed: 10698648]

102. Kogan F, Haris M, Debrosse C, Singh A, Nanga RP, Cai K, Hariharan H, Reddy R. *In vivo* chemical exchange saturation transfer imaging of creatine (CrCEST) in skeletal muscle at 3T. J Magn Reson Imaging. 2014; 40:596–602. [PubMed: 24925857]

103. Wu RH, Longo DL, Aime S, Sun PZ. Quantitative description of radiofrequency (RF) power-based ratiometric chemical exchange saturation transfer (CEST) pH imaging. NMR Biomed. 2015; 28:555–565. [PubMed: 25807919]

104. Pumphrey A, Yang ZS, Ye SJ, Powell DK, Thalman S, Watt DS, Abdel-Latif A, Unrine J, Thompson K, Fornwalt B, et al. Advanced cardiac chemical exchange saturation transfer

(cardioCEST) MRI for *in vivo* cell tracking and metabolic imaging. NMR Biomed. 2016; 29:74–83. [PubMed: 26684053]

105. Cai K, Haris M, Singh A, Kogan F, Greenberg JH, Hariharan H, Detre JA, Reddy R. Magnetic resonance imaging of glutamate. Nat Med. 2012; 18:302–306. [PubMed: 22270722]
106. Chan KWY, Jiang L, Cheng ML, Wijnen JP, Liu GS, Huang P, van Zijl PCM, McMahon MT, Glunde K. CEST-MRI detects metabolite levels altered by breast cancer cell aggressiveness and chemotherapy response. NMR Biomed. 2016; 29:806–816. [PubMed: 27100284]
107. Jin T, Autio J, Obata T, Kim SG. Spin-locking versus chemical exchange saturation transfer MRI for investigating chemical exchange process between water and labile metabolite protons. Magn Reson Med. 2011; 65:1448–1460. [PubMed: 21500270]
108. Aime S, Calabi L, Biondi L, De Miranda M, Ghelli S, Paleari L, Rebaudengo C, Terreno E. Iopamidol: exploring the potential use of a well-established X-ray contrast agent for MRI. Magn Reson Med. 2005; 53:830–834. [PubMed: 15799043]
109. Longo DL, Dastru W, Digilio G, Keupp J, Langereis S, Lanzardo S, Prestigio S, Steinbach O, Terreno E, Uggeri F, et al. Iopamidol as a responsive MRI-chemical exchange saturation transfer contrast agent for pH mapping of kidneys: *in vivo* studies in mice at 7 T. Magn Reson Med. 2011; 65:202–211. [PubMed: 20949634]
110. Yang X, Song X, Ray Banerjee S, Li Y, Byun Y, Liu G, Bhujwalla ZM, Pomper MG, McMahon MT. Developing imidazoles as CEST MRI pH sensors. Contrast Media Mol Imaging. 2016; 11:304–312. [PubMed: 27071959]
111. Bar-Shir A, Liu GS, Liang YJ, Yadav NN, McMahon MT, Walczak P, Nimmagadda S, Pomper MG, Tallman KA, Greenberg MM, et al. Transforming thymidine into a magnetic resonance imaging probe for monitoring gene expression. J Am Chem Soc. 2013; 135:1617–1624. [PubMed: 23289583]
112. Yang X, Song X, Li Y, Liu G, Ray Banerjee S, Pomper MG, McMahon MT. Salicylic acid and analogues as diaCEST MRI contrast agents with highly shifted exchangeable proton frequencies. Angew Chem Int Ed Engl. 2013; 52:8116–8119. [PubMed: 23794432]
113. Song X, Walczak P, He X, Yang X, Pearl M, Bulte JW, Pomper MG, McMahon MT, Janowski M. Salicylic acid analogues as chemical exchange saturation transfer MRI contrast agents for the assessment of brain perfusion territory and blood–brain barrier opening after intra-arterial infusion. J Cereb Blood Flow Metab. 2016; 36:1186–1194. [PubMed: 26980755]
114. Yang X, Yadav NN, Song X, Ray Banerjee S, Edelman H, Minn I, van Zijl PC, Pomper MG, McMahon MT. Tuning phenols with Intra-Molecular bond Shifted HYdrogens (IM-SHY) as diaCEST MRI contrast agents. Chemistry. 2014; 20:15824–15832. [PubMed: 25302635]
115. Li JK, Feng XX, Zhu W, Oskolkov N, Zhou TH, Kim BK, Baig N, McMahon MT, Oldfield E. Chemical exchange saturation transfer (CEST) agents: quantum chemistry and MRI. Chem Eur J. 2016; 22:264–271. [PubMed: 26616530]
116. Lesniak WG, Oskolkov N, Song X, Lal B, Yang X, Pomper M, Laterra J, Nimmagadda S, McMahon MT. Salicylic acid conjugated dendrimers are a tunable, high performance CEST MRI Nano-Platform. Nano Lett. 2016; 16:2248–2253. [PubMed: 26910126]
117. Aime S, Barge A, Delli Castelli D, Fedeli F, Mortillaro A, Nielsen FU, Terreno E. Paramagnetic lanthanide(III) complexes as pH-sensitive chemical exchange saturation transfer (CEST) contrast agents for MRI applications. Magn Reson Med. 2002; 47:639–648. [PubMed: 11948724]
118. Zhang SR, Winter P, Wu KC, Sherry AD. A novel europium(III)-based MRI contrast agent. J Am Chem Soc. 2001; 123:1517–1518. [PubMed: 11456734]
119. Banci, L., Bertini, I., Luchinat, C. Nuclear and Electron Relaxation. Weinheim, Germany: VCH; 1991.
120. Peters JA, Huskens J, Raber DJ. Lanthanide induced shifts and relaxation rate enhancements. Prog Nucl Magn Reson Spectrosc. 1996; 28:283–350.
121. Viswanathan S, Kovacs Z, Green KN, Ratnakar SJ, Sherry AD. Alternatives to gadolinium-based MRI metal chelates. Chem Rev. 2010; 110:2960–3018. [PubMed: 20397688]
122. Helm L, Merbach AE. Inorganic and bioinorganic solvent exchange mechanisms. Chem Rev. 2005; 105:1923–1959. [PubMed: 15941206]

123. Dorazio SJ, Olatunde AO, Tsitovich PB, Morrow JR. Comparison of divalent transition metal ion para-CEST MRI contrast agents. J Biol Inorg Chem. 2014; 19:191–205. [PubMed: 24253281]

124. Winter PM, Cai KJ, Chen J, Adair CR, Kiefer GE, Athey PS, Gaffney PJ, Buff CE, Robertson JD, Caruthers SD, et al. Targeted PARACEST nanoparticle contrast agent for the detection of fibrin. Magn Reson Med. 2006; 56:1384–1388. [PubMed: 17089356]

125. Terreno E, Cabella C, Carrera C, Castelli DD, Mazzon R, Rollet S, Stancanello J, Visigalli M, Aime S. From spherical to osmotically shrunken paramagnetic liposomes: an improved generation of LIPOCEST MRI agents with highly shifted water protons. Angew Chem Int Ed. 2007; 46:966–968.

126. Pikkemaat JA, Wegh RT, Lamerichs R, van de Molengraaf RA, Langereis S, Burdinski D, Raymond AYF, Janssen HM, de Waal BFM, Willard NP, et al. Dendritic PARACEST contrast agents for magnetic resonance imaging. Contrast Media Mol Imaging. 2007; 2:229–239. [PubMed: 17937448]

127. Ali MM, Yoo B, Pagel MD. Tracking the relative *in vivo* pharmacokinetics of nanoparticles with PARACEST MRI. Mol Pharm. 2009; 6:1409–1416. [PubMed: 19298054]

128. Ali MM, Bhuiyan MPI, Janic B, Varma NRS, Mikkelsen T, Ewing JR, Knight RA, Pagel MD, Arbab AS. A nano-sized PARACEST-fluorescence imaging contrast agent facilitates and validates *in vivo* CEST MRI detection of glioma. Nanomedicine. 2012; 7:1827–1837. [PubMed: 22891866]

129. Ruiz-Cabello J, Barnett BP, Bottomley PA, Bulte JW. Fluorine (19F) MRS and MRI in biomedicine. NMR Biomed. 2011; 24:114–129. [PubMed: 20842758]

130. Ahrens ET, Helfer BM, O'Hanlon CF, Schirda C. Clinical cell therapy imaging using a perfluorocarbon tracer and fluorine-19 MRI. Magn Reson Med. 2014; 72:1696–1701. [PubMed: 25241945]

131. Rose LC, Kadayakkara DK, Wang G, Bar-Shir A, Helfer BM, O'Hanlon CF, Kraitchman DL, Rodriguez RL, Bulte JW. Fluorine-19 labeling of stromal vascular fraction cells for clinical imaging applications. Stem Cells Transl Med. 2015; 4:1472–1481. [PubMed: 26511652]

132. Srinivas M, Turner MS, Janjic JM, Morel PA, Laidlaw DH, Ahrens ET. *In vivo* cytometry of antigen-specific t cells using 19F MRI. Magn Reson Med. 2009; 62:747–753. [PubMed: 19585593]

133. Bulte JW. Hot spot MRI emerges from the background. Nat Biotechnol. 2005; 23:945–946. [PubMed: 16082363]

134. Chechik V, Crooks RM. Dendrimer-encapsulated Pd nanoparticles as fluorous phase-soluble catalysts. J Am Chem Soc. 2000; 122:1243–1244.

135. Cooper AI, Londono JD, Wignall G, McClain JB, Samulski ET, Lin JS, Dobrynin A, Rubinstein M, Burke ALC, Frechet JMJ, et al. Extraction of a hydrophilic compound from water into liquid CO_2 using dendritic surfactants. Nature. 1997; 389:368–371.

136. Jiang Z-X, Liu X, Jeong E-K, Yu YB. Symmetry-guided design and fluorous synthesis of a stable and rapidly excreted imaging tracer for 19F MRI. Angew Chem Int Ed. 2009; 48:4755–4758.

137. Yu WJ, Yang YQ, Bo SW, Li Y, Chen SZ, Yang ZG, Zheng X, Jiang ZX, Zhou X. Design and synthesis of fluorinated dendrimers for sensitive F-19 MRI. J Org Chem. 2015; 80:4443–4449. [PubMed: 25849491]

138. Bo SW, Song C, Li Y, Yu WJ, Chen SZ, Zhou X, Yang ZG, Zheng X, Jiang ZX. Design and synthesis of fluorinated amphiphile as F-19 MRI/fluorescence dual-imaging agent by tuning the self-assembly. J Org Chem. 2015; 80:6360–6366. [PubMed: 26016450]

139. Ogawa M, Kataoka H, Nitahara S, Fujimoto H, Aoki H, Ito S, Narazaki M, Matsuda T. Water-soluble fluorinated polymer nanoparticle as 19F MRI contrast agent prepared by living random copolymerization from dendrimer initiator. Bull Chem Soc Jpn. 2011; 85:79–86.

140. Yu W, Yang Y, Bo S, Li Y, Chen S, Yang Z, Zheng X, Jiang ZX, Zhou X. Design and synthesis of fluorinated dendrimers for sensitive (19)F MRI. J Org Chem. 2015; 80:4443–4449. [PubMed: 25849491]

141. Xiao Q, Rubien JD, Wang Z, Reed EH, Hammer DA, Sahoo D, Heiney PA, Yadavalli SS, Goulian M, Wilner SE, et al. Self-sorting and coassembly of fluorinated, hydrogenated, and hybrid Janus

dendrimers into dendrimersomes. J Am Chem Soc. 2016; 138:12655–12663. [PubMed: 27580315]

142. Wang Z, Yue X, Wang Y, Qian C, Huang P, Lizak M, Niu G, Wang F, Rong P, Kiesewetter DO, et al. A symmetrical fluorous dendron-cyanine dye-conjugated bimodal nanoprobe for quantitative 19F MRI and NIR fluorescence bioimaging. Adv Healthc Mater. 2014; 3:1326–1333. [PubMed: 24789108]
143. Malik N, Wiwattanapatapee R, Klopsch R, Lorenz K, Frey H, Weener JW, Meijer EW, Paulus W, Duncan R. Dendrimers: relationship between structure and biocompatibility *in vitro*, and preliminary studies on the biodistribution of 125I-labelled polyamidoamine dendrimers *in vivo*. J Control Release. 2000; 65:133–148. [PubMed: 10699277]
144. Kobayashi H, Kawamoto S, Jo SK, Bryant HL Jr, Brechbiel MW, Star RA. Macromolecular MRI contrast agents with small dendrimers: pharmacokinetic differences between sizes and cores. Bioconjug Chem. 2003; 14:388–394. [PubMed: 12643749]
145. Ihre HR, De Jesus OLP, Szoka FC, Frechet JMJ. Polyester dendritic systems for drug delivery applications: design, synthesis, and characterization. Bioconjug Chem. 2002; 13:443–452. [PubMed: 12009932]
146. Grinstaff MW. Biodendrimers: new polymeric biomaterials for tissues engineering. Chem Eur J. 2002; 8:2838–2846.
147. Gerretsen SC, Versluis B, Bekkers S, Leiner T. Cardiac cine MRI: comparison of 1.5 T, non-enhanced 3.0 T and blood pool enhanced 3. 0 T imaging. Eur J Radiol. 2008; 65:80–85. [PubMed: 18155867]

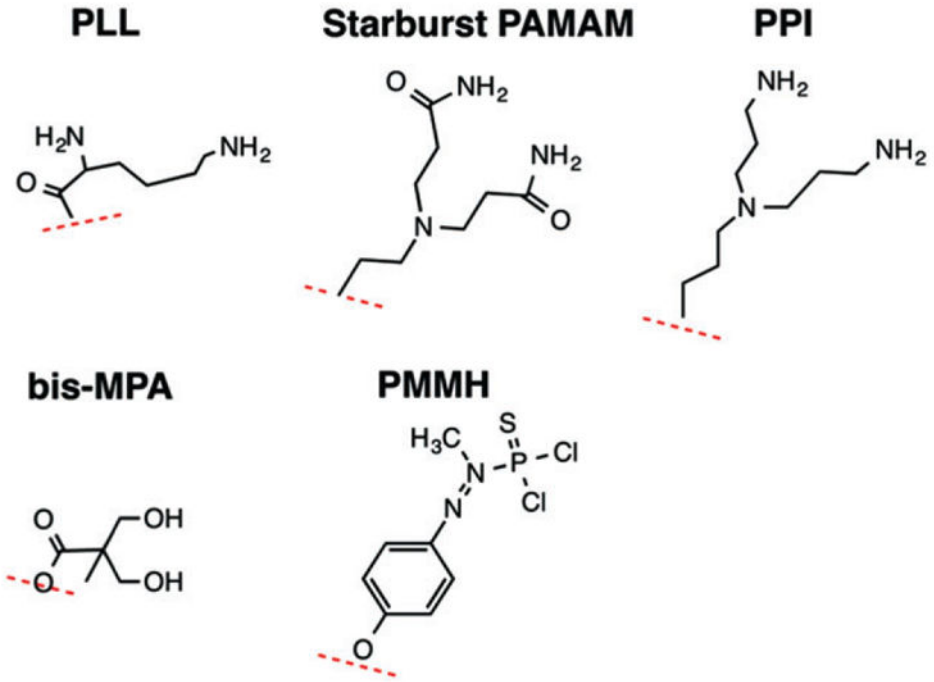

FIGURE 1.

Building blocks that have been used for production of commercially available dendrimers. These include poly-L-lysine (PLL), polyaminoamine (PAMAM), polypropylimine [PPI, also known as diaminobutane (DAB)], 2,2-bis-methylolpropionic acid (bis-MPA), and phenoxymethyl(methylhydrazone) (PMMH).

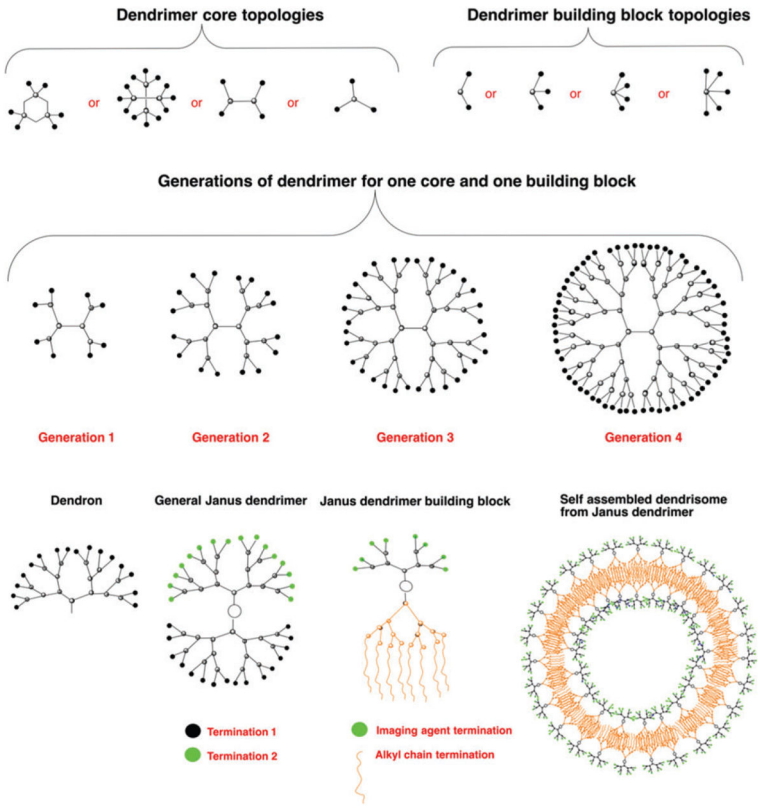

FIGURE 2.

Available topologies for synthesizing dendrimers. Shown are representative core and building block topologies (top row), the topology for Generations 1–4 for one core and one building block as present in polyaminoamine (PAMAM) and poly-L-lysine (PLL) dendrimers (middle row), and a topology for a dendron, a generalized Janus dendrimer with two dendrons presenting different terminal groups which are grafted to a single core, a Janus dendrimer suitable for self-assembly into MR dendrisomes, and an MR dendrisome (bottom row).

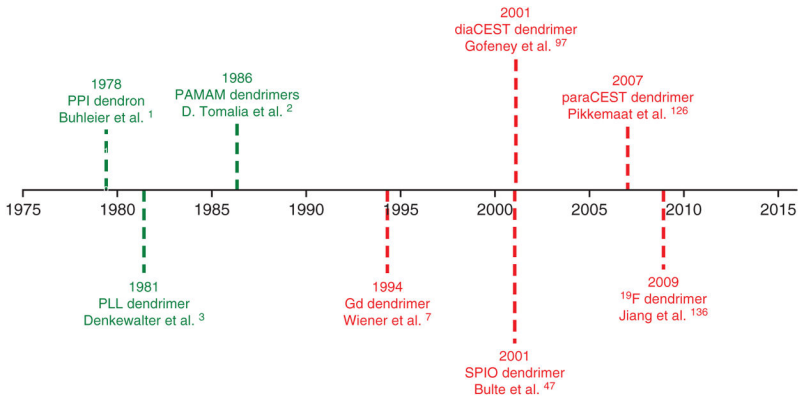

FIGURE 3.

Chronological representation of milestone publications on dendrimer development and their (green) use as MRI agents (red).

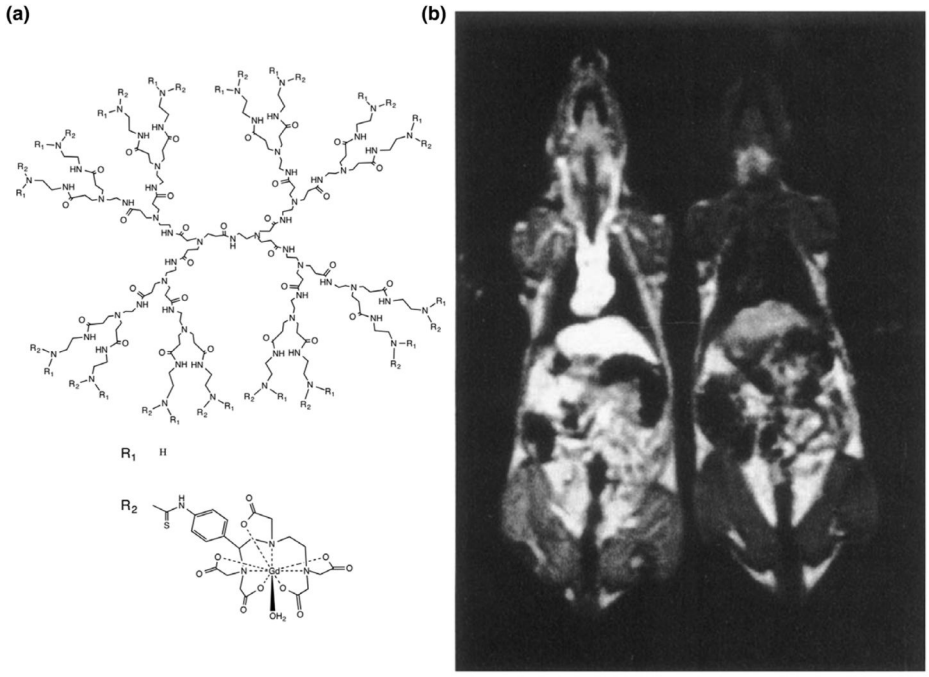

FIGURE 4.

The first dendrimer platform used as MR contrast agent. (a) General structure of PAMAM-Gd-DOTA dendrimers showing a G = 3PAMAM dendrimer and Gd-DOTA with linker. (b) The first image acquired with PAMAM Gd-DOTA dendrimers as MR contrast agent. A Gd-DOTA-conjugated G = 6 PAMAM dendrimer, having a half-life of approximately 200 min, was injected in the left rat at 0.005 mmol Gd kg^{-1}. A clear vascular enhancement can be seen compared with the uninjected rat on the right. (Reprinted with permission from Ref 7 Copyright 1994 John Wiley & Sons, Inc.)

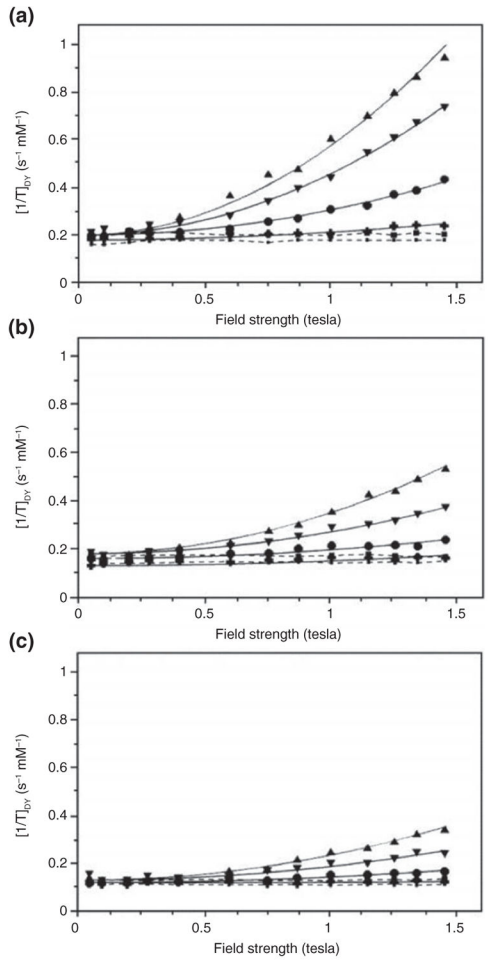

FIGURE 5.

Variable field relaxometry of a Dy-DOTA-conjugated G = 5 PAMAM dendrimer and single Dy(III) chelates. Shown are the T_2 relaxivities of (a) Dy-DOTA-PAMAM G = 5 dendrimers, (b) Dy-DOTA single chelates, and (c) Dy-DTPA single chelates as a function of magnetic field strength. Data are shown at 3 (▲), 10 (▼), 20 (●), and 37°C (+). Solid lines represent quadratic fits to the equation $1/T_2 = a + bB_0,^2$ with B_0 being the external magnetic field strength. For comparison, the T_1 relaxivities are negligible, shown as dashed lines at 3 (■) and 37 C (·). (Reprinted with permission form Ref 44 Copyright 1998 Wolters Kluwer Health)

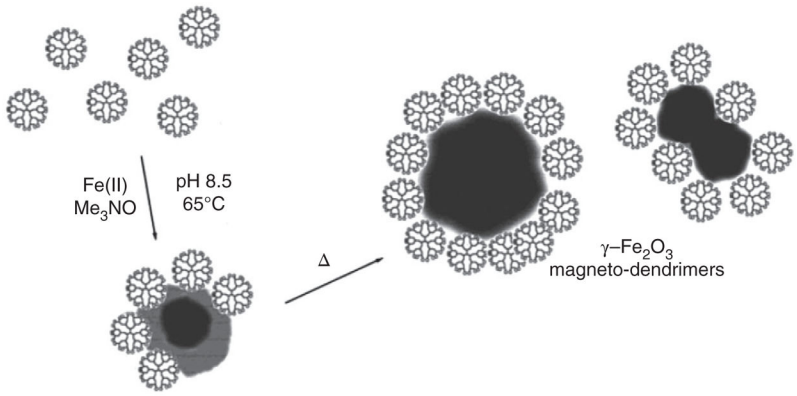

FIGURE 6.

Structure of magnetodendrimers. Shown is a schematic representation of the stabilization of maghemite nanoparticles by G = 4.5 carboxyl-terminated PAMAM dendrimers. (Reprinted with permission from Ref 48 Copyright 2001 American Chemical Society)

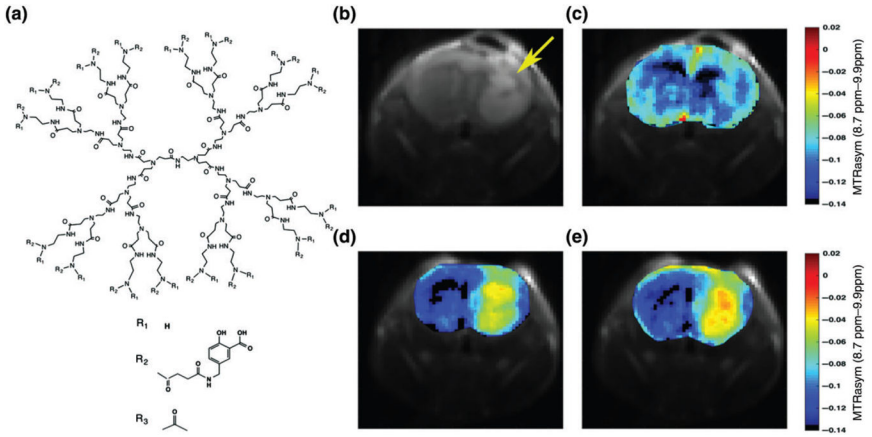

FIGURE 7.

(a) General structure of PAMAM-SA-Ac dendrimers showing a G = 3PAMAM dendrimer, salicylic acid (SA) with linker, and acetyl termination. (B–E) In vivo images of salicylic acid methyl ester (SAME) G = 5 PAMAM dendrimer conjugates infused into a mouse carrying a glioblastoma xenograft. Shown are (b) T_{2w} (arrow highlights tumor) and CEST MR images obtained (c) pre- and (d) 30 and (e) 60 min postinjection of a 500 μM solution of diaCEST dendrimer. (Reprinted with permission from Ref 116 Copyright 2016 American Chemical Society)

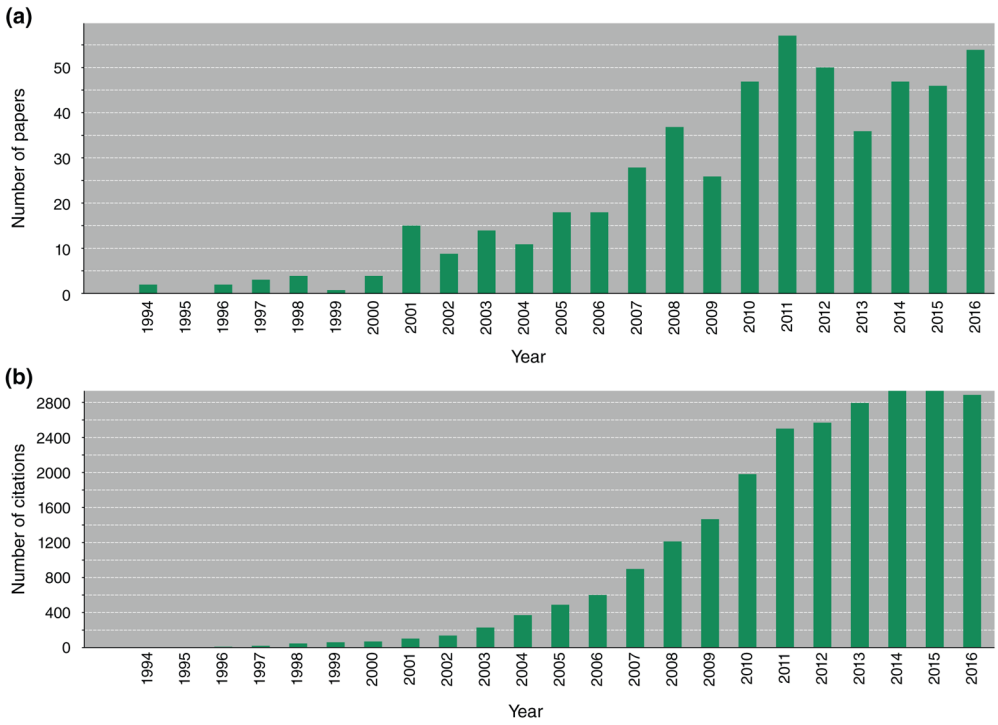

FIGURE 8.

Two decades of (a) publications and (b) citations on dendrimer MRI agents (Source: ISI Web of Science).